Ultramicroscopy 110 (2010) 694–700

Contents lists available at ScienceDirect

Ultramicroscopy

journal homepage: www.elsevier.com/locate/ultramic

Kinetics of interaction of HIV fusion protein (gp41) with lipid membranes studied by real-time AFM imaging

Arkady Bitler [a,*], Naama Lev [b], Yael Fridmann-Sirkis [b], Lior Blank [b], Sidney R. Cohen [a], Yechiel Shai [b]

[a] Department of Chemical Research Support, Israel
[b] Department of Biological Chemistry, Weizmann Institute of Science, Rehovot 76100, Israel

ARTICLE INFO

Keywords:
AFM
Fusion peptide
gp41
Membrane destruction
Kinetics

ABSTRACT

One of the most important steps in the process of viral infection is a fusion between cell membrane and virus, which is mediated by the viral envelope glycoprotein. The study of activity of the glycoprotein in the post-fusion state is important for understanding the progression of infection. Here we present a first real-time kinetic study of the activity of gp41 (the viral envelope glycoprotein of human immunodeficiency virus—HIV) and its two mutants in the post-fusion state with nanometer resolution by atomic force microscopy (AFM). Tracking the changes in the phosphatidylcholine (PC) and phosphatidylcholine–phosphatidylserine (PC:PS) membrane integrity over one hour by a set of AFM images revealed differences in the interaction of the three types of protein with zwitterionic and negatively charged membranes. A quantitative analysis of the slow kinetics of hole formation in the negatively charged lipid bilayer is presented. Specifically, analysis of the rate of roughness change for the three types of proteins suggests that they exhibit different types of kinetic behavior.

1. Introduction

Application of atomic force microscopy (AFM) to studies of biological systems has a few important advantages over other techniques such as electron microscopy. These include: (i) the ability to produce reliable results – both images and measurements of physical characteristics of the studied surfaces – in liquid environment, including buffers with high salt concentration, (ii) the ability to achieve nanoscale resolution under these conditions, (iii) the extreme surface sensitivity of the technique, and (iv) the ability to track changes of the biological system in real time. These advantages have positioned AFM as a powerful tool for studying processes in biological specimens at high resolution [1,2]. During the last decade there has been a wealth of studies applying AFM for imaging various lipid bilayers and their interactions with peptides and proteins [3–12].

The initial step of viral infection is frequently mediated by viral envelope proteins [13,14]. In the case of the human immunodeficiency virus (HIV) the envelope protein forms a trimer, with each monomer consisting of two non-covalently associated subunits, gp120 the receptor binding domain, and gp41 which is responsible for the mixing of the viral and target cell membrane leading to membrane fusion [15]. Binding of gp120 to the corresponding target membrane receptor triggers a cascade of conformational changes in the envelope protein. This results in fusion induction of the viral envelope with the target membrane, thereby initiating infection by the virus [17–21]. As a consequence of the conformational changes, the N-terminus of gp41 becomes exposed and interacts with the target cell membrane. This creates a prehairpin intermediate (PHI) that bridges both viral and cellular membranes [16,22]. The PHI is short lived, and collapses after up to 30 min into a low-energy conformation of a six helix bundle (SHB) [23,24]. However, recent studies revealed that: (i) other regions within gp41 could be involved in membrane destabilization and fusion [25–35] and (ii) formation of holes starts before gp41 folding to SHB is complete [36]. Moreover association of gp41 with negatively charged membranes was shown to cause structural modifications and as a consequence influence SHB stability [35]. In contrast, the SHB interaction with a zwiterionic membrane did not cause its dissociation [31]. Recently, we reported investigation of the biochemical and structural aspects of these issues with AFM [37]. The previous study examined final states of the perturbed membrane to deduce the contribution of all the functional regions within gp41 to the structural and functional properties of the protein and conversely the influence of the membrane on the structure and core stability of gp41.

In spite of the vast amount of information acquired over the past two decades on HIV envelope proteins and their interactions

* Corresponding author at: Weizmann Institute of Science, P.O. Box 26, Rehovot 76100, Israel. Tel.: +972 8 9346207; fax: +972 8 9342703.
E-mail address: arkady.bitler@weizmann.ac.il (A. Bitler).

0304-3991/$ - see front matter © 2010 Elsevier B.V. All rights reserved.
doi:10.1016/j.ultramic.2010.02.034

with lipid membranes, kinetic studies exploiting the high resolution visualization of interactions between lipid membranes and gp41 ectodomain by AFM have never been reported. In this work we present a direct observation of the interaction between gp41 and its two truncated versions and supported lipid bilayers of two types: zwitterionic and negatively charged. The studies were done in liquid buffer by AFM in real time with nanoscale resolution. Quantitative analysis of the real-time studies allows characterization of the kinetics of membrane destruction for the three types of proteins. Significant differences in the time course for the interaction between the lipid bilayer and different truncated forms of gp41 are revealed.

2. Materials and methods

2.1. Materials

LPC and PC (from egg yolk) were obtained from Sigma. LPS and PS (from porcine brain) were obtained from Avanti. *N*-(lissamine rhodamine B sulfonyl) dioleoylphsphatidylethanolamine (Rho-PE) and *N*-(7-nitrobenz-2-oxa-1,3-diazol-4-yl) dioleophosphatidylethanolamine (NBDPE) were purchased from Molecular Probes (Eugene, OR). All other reagents were of analytical grade.

2.2. HIV-1 gp41 ectodomain cloning, expression, and purification

Gp41 from the HIV-1 strain HXB2 was cloned into pET24d plasmid between HindIII and BamHI sites. For this, the intrinsic HindIII site was cancelled by directed mutagenesis. Also the two cysteins in the loop were mutated to alanines. The sequence of the ectodomain starts from 512 to 684, the sequence of e-core starts from 546 to 684 and the sequence of the core starts from 538 to 666. Asparagine and glycine were inserted between TrpdelE and gp41 for future nonenzymatic cleavage. The proteins were expressed in BL21 pLys S *E. Coli* by growing cell culture in LB supplemented with kanamycin until OD600 was at 0.4. Then 1 mM of IPTG was added to induce expression. The chimeras were located in inclusion bodies and were purified by sonicating the cells, centrifuged at 15,500 rpm and 4 °C for 30 min, following washing the inclusion bodies 6 times with lysis buffer (50 mM Tris, pH 7.0, 100 mM NaCl, 5 mM EDTA, 0.1 mM PMSF, 0.1% triton-100). The purified chimeras were then nonenzymatically cleaved by hydroxylamine between asparagine and glycine. The products of the reactions were separated by RP-HPLC at 80 °C using C18 column and a gradient of 25–80% acetonitrile in water for 40 min. The eluted proteins were dialyzed for 24 h against 50 mM sodium formate buffer (pH 3) at 4 °C using a 3 kDa cutoff dialysis cassette. The dialyzed proteins were concentrated by centrikones and verified by mass spectrometry. The construct of the core was treated differently as it was in the soluble fraction of the cell. In short, cells were lysed in the presence of glacial acetic acid (as previously described).

2.3. Preparation of large unilamellar vesicles

Thin films of PC or PC:PS (3:2) were generated following dissolution of the lipids in a 2:1 (v/v) mixture of $CHCl_3$/MeOH and then dried under a stream of nitrogen while rotating. Two populations of films were generated: (1) lipid only mixtures, termed unlabeled, and (2) the same lipid mixture containing 0.6% molar of NBD-PE and RHO-PE each, termed labeled. The films were lyophilized overnight, sealed with argon gas to prevent oxidation, and stored at −20 °C. Before the experiment, the films were suspended in PBS buffer −/− (without Ca^{++} and Mg^{++}) and vortexed for 1.5 min. The lipid suspension underwent five cycles of freezing–thawing and then extrusion through polycarbonate membranes with 1 and 0.1 μm diameter pores to create LUVs as imaged by negative staining electron microscopy.

2.4. Preparation of supported lipid bilayers for atomic force microscopy (AFM)

Supported lipid bilayers were prepared using the vesicle fusion method. Briefly, PC and PC:PS (3:2) LUV suspensions (1 mM, 70 μl) were deposited onto freshly cleaved mica squares (1 cm^2) and allowed to adsorb and fuse on the solid surface for 4 h at 25 °C. Samples were then placed in AFM.

2.5. AFM experiments

Supported bilayers were investigated using a MultiMode AFM with Nanoscope V controller (Veeco Metrology LLC, Santa Barbara, CA) equipped with a small scanner (E-scanner). AFM images were obtained in tapping mode in buffer solution at room temperature (23–25 °C). The stability of the membrane under our scanning conditions was initially verified by recording a long (45–60 min, 10–12 images) series of images before protein injection. The AFM probe was withdrawn by 150–200 nm during protein injection to avoid any damage due to local turbulence and ensure tracking was maintained in the same area. The scanning was resumed approximately 5 min after protein injection (defined as time 0) and continued for an equivalent time as the series made before the injection. In addition, a 'reference point' e.g., small but distinct membrane corrugation was tracked before and after protein injection to verify that the same area was scanned. The proteins were dissolved in 50 mM sodium formate buffer (pH 3). Next, they were injected into the buffer to reach approximately 0.9 μM protein concentration, and images were taken continually every ~3–5 min. All images were recorded using oxide-sharpened microfabricated Si_3N_4 cantilevers (DNP-S, Veeco Metrology, Santa Barbara, CA) with a spring constant of ~0.12 N/m (manufacturer specified) and at a scan rate of 1.5–3.5 Hz. The target amplitude was 300 mV (~22 nm) and set point was 245–250 mV (~18 nm) for all measurements (to avoid possible influence of different penetration depths on the process of membrane destruction by the tested proteins). Therefore 'light' tapping has been applied to avoid possible damage to the membranes and influence of the scanning itself on the membrane destruction produced by the gp41 and the two mutants in the case of PC:PS lipids.

2.6. Image analysis

The original images were opened, processed and roughness was evaluated by a custom Matlab code (Matlab V. 7.6.0.324; MathWorks Inc., Natick, MA). Moreover the program allows dividing the original image to a predefined number of sub-images, making roughness evaluation for each part. The program could work also in the batch mode that enables fast processing of the image set.

3. Results

3.1. Interaction of gp41 and its two truncated forms with zwitterionic membrane

Corresponding triplets of 3D images (for three types of protein: gp41 and the two mutants) appear in our previous publication

[37]. Comparison of successive images during the period *before* the protein injection proves that in all cases no membrane perturbations were produced by the scanning itself. Inspection of successive images during the period *after* protein injections proves that for all three proteins, no membrane perturbations occurred: rms roughness remained essentially unchanged over 50 min of scanning before and 50 min after protein injection, lying in the range of 0.18–0.22 nm (rms). These data yield additional proof that gp41 and the two mutants do not affect the PC lipid membrane integrity.

3.2. Interaction of gp41 and its two truncated forms with negatively charged membrane

Corresponding triplets of 3D images (for three types of protein: gp41 and the two mutants) could also be found in our previous publication [37]. As for the previous case, comparison of successive images during the period *before* injection of gp41 and the two mutants proves that no membrane perturbations were produced by the scanning itself. These roughness values ranged between 0.19 and 0.32 nm (rms) with no observable trend occurring over the scanning time. In contrast to the case of the zwitterionic membrane, changes in the PC:PS membrane topography begin appearing even in the first image after injection of each of the 3 proteins (gp41 and its two mutants), and the changes continue throughout the course of the run.

3.3. Topography changes of phosphatidylcholine–phosphatidylserine (PC:PS) membrane in the process of interaction with gp41 and the two mutants

Neither full length protein gp41, nor the two mutants altered the topography of the PC lipid membrane. In contrast, all three types of proteins significantly perturb the state of the PC:PS membrane, but the mechanism appears to be different. With the core and ecto-domain, a few small holes appear in the PC:PS membrane at the early stages of reaction. The typical depth of these holes is 2 nm, but some holes are only 1 nm deep. Typical images and cross-sections are presented in Figs. 1 and 2. In contrast to this the e-core protein produces wider and deeper holes (depth up to 3 nm) within 15 min after e-core injection. A typical image is presented in Fig. 3. Moreover elevated domains of about 3 nm height start to appear near the edges of the holes at the initial stage of e-core action. The differences are intensified in the later stages of the reaction. PC:PS membranes pretreated with

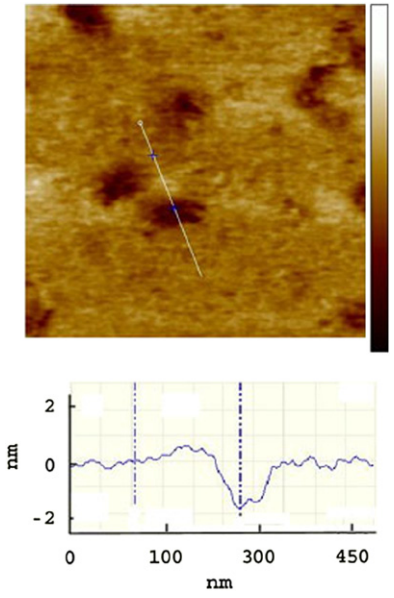

Fig. 1. Typical image of the interaction between core mutant and PC:PS bilayer immediately after protein addition (1 μm × 1 μm; *z* scale: 5 nm). Cross-section shows the depth of hole at the initial stage (~2 nm) and approximate width of hole (~50 nm). Cross-section is shown in the image as white line.

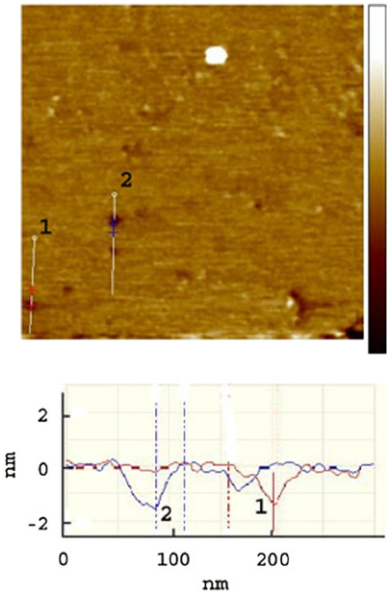

Fig. 2. Typical image of the interaction between full length ectodomain and PC:PS bilayer (1 μm × 1 μm; *z* scale: 5 nm) immediately after protein addition. Cross-sections show the depth of holes at the initial stage (~2 nm) and approximate width of hole (~20 nm). The positions of the cross-sections are marked on the image by lines 1 and 2.

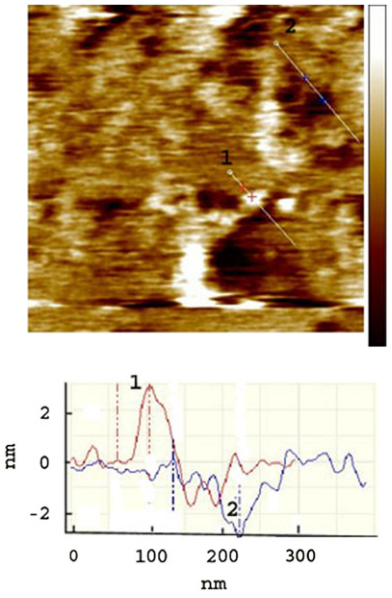

Fig. 3. Typical image of the interaction between e-core mutant and PC:PS bilayer (1 μm × 1 μm; *z* scale: 5 nm) immediately after protein addition. Cross-sections show the depths of holes at the initial stage (~2 nm) and approximate widths of holes (~80–120 nm). Cross-section is shown in the image as lines 1 and 2. This image reveals the appearance of the membrane elevations at the initial stage for the e-core mutant (cross-section 1).

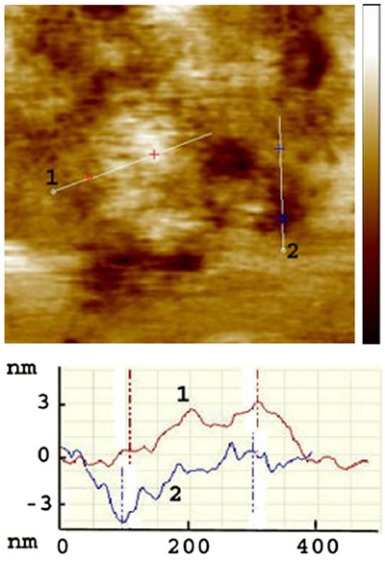

Fig. 4. Typical image of the final stage (40 min) of the interaction between core mutant and PC:PS bilayer (1 μm × 1 μm; *z* scale: 10 nm—twice that of Figs. 1–3). Cross-sections show the depths of holes at the final stage (~4 nm) and approximate widths of holes. The cross-section positions are seen in the image—lines 1 and 2. The membrane protrusions appear over the entire membrane at the final stage.

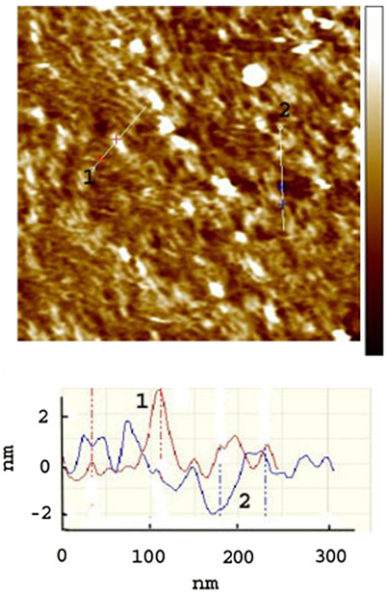

Fig. 5. Final stage (40 min) of the interaction between ectodomain and PC:PS bilayer (1 μm × 1 μm; *z* scale: 5 nm). This image reveals that the membrane is fully covered by relatively small corrugations. Cross-sections show the depths of holes at the final stage (~4 nm) and approximate widths of holes. Cross-section positions are shown on image as white lines 1 and 2. The ubiquitous nature of the mesh in the final stage prevents a choice of zero-level (corresponding to the unperturbed membrane).

core mutant exhibit medium size holes of 4 nm depth and elevated domains of 2–3 nm height 45–50 min after injection (Fig. 4). In this later stage, PC:PS membranes pretreated with ecto-domain exhibit a strongly corrugated surface with many small holes and small elevated domains with heights of about 2–3 nm (Fig. 5). In contrast action of the e-core mutant after long times results in very large holes of 4 nm depth and elevated domains of up to 8 nm height (Fig. 6).

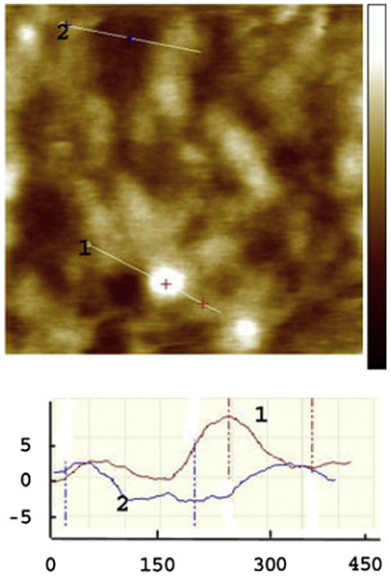

Fig. 6. Typical image of the final stage (40 min) of the interaction between e-core mutant and PC:PS bilayer (1 μm × 1 μm; *z* scale: 15 nm—note larger scale than in previous images). Cross-sections show the depths of holes at the final stage (~4 nm) and approximate widths of holes. Placement of cross-sections noted as lines 1 and 2 in the image. Very large membrane protrusions and wide holes cover the whole membrane at the final stage preventing a choice of zero-level (corresponding to the flat membrane).

3.4. Kinetics of membrane reorganization during interaction with gp41 and the two mutants with PC:PS membrane

Membrane perturbations or destruction can be characterized quantitatively in different ways. Here we suggest comparing the root mean square (rms) roughness as quantitative parameter of membrane deviation from the flat surface. This parameter is a measure of the spread of height values around a mean. For a Gaussian distribution of heights, this parameter is approximately 1/3 the difference between the 5th and 95th percentile of represented heights [38]. Analyzing with this parameter the sets of images acquired over about 45–50 min enables a quantification of the time course or kinetics of the changes of the membrane state. Corresponding graphs for PC:PS membranes treated by e-core, ecto-domain and core proteins are presented in Fig. 7(a), (b) and (c), respectively. It is clear that PC:PS membrane, treated with core mutant, exhibits a slow, almost linear increase in the membrane roughness over about 50 min. The action of the ecto-domain (or full gp41 protein), exhibits an apparent acceleration in the time interval between 5 and 15 min. But roughness changes of PC:PS membrane, treated with e-core mutant, undergoes a steep increase in the same time interval between 5 and 15 min. The rate of roughness change can be associated with the rate of membrane destruction. The large perturbations seen in this early period indicate that the major action occurs early in the process. Comparison of the curves for the different mutants enables us to quantify the 'effectiveness' of each applied protein. One can conclude that the e-core mutant is even more 'effective', than the full ecto-domain and much more effective than the core mutant.

4. Discussion

The unique possibility to explore organization of supported lipid bilayers in liquid environment by AFM enables visualization of the interaction of protein gp41 and its mutants in real time. Moreover it provides the possibility to obtain information about

details of this process at the nanometer scale. Inspection of the series of images obtained and comparison of the series for intact gp41 ectodomain and the two mutants allow characterizing different ways in which these proteins interact with lipid bilayers.

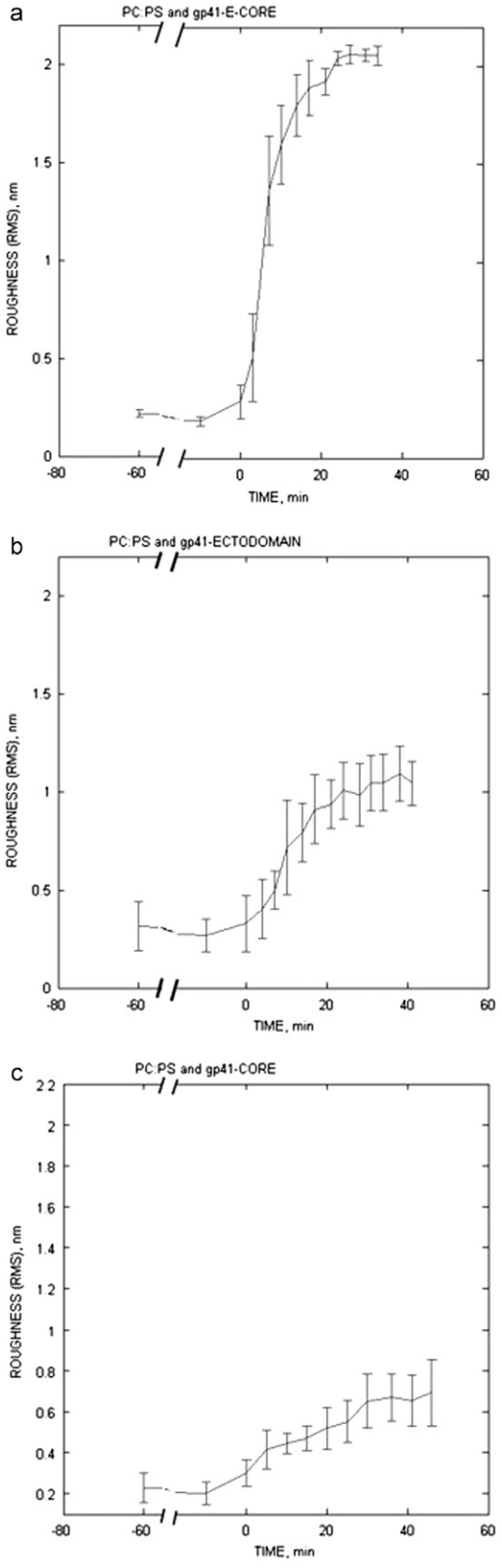

Firstly—the three types of protein have no effect on the phosphatidylcholine (PC) membrane integrity. Therefore one can conclude that neither the six helix bundle folded form of the intact gp41 ectodomain, nor those of the two mutants interact with zwitterionic membranes. Secondly—in contrast to this the PC:PS lipid bilayers are extensively modified by all three proteins, but seemingly by different mechanisms. In the initial stage of the interaction of core mutant with a PC:PS membrane a few relatively wide (about 50 nm) holes appear, with small (less than 1 nm) elevations of the membrane near the hole edges. The depths of these holes are about 2 nm which is consistent with removal of half of the bilayer (see Fig. 1). In this case the elevations can be assigned to lipid molecules which were removed from the membrane, and subsequently accumulated near the edge of the hole, lying horizontally rather than assuming a vertical head–tail orientation. At the initial stage of the interaction of ecto-domain (full gp41) with PC:PS membrane a few but narrow holes appear (15–25 nm—2–3 times narrower than in the case of core mutant). The depths of these holes are also about 2 nm (half of a bilayer—see Fig. 2). However, in this case the elevations appear as small corrugations of the lipid bilayer surface and appear far from the edges of the holes (see for example upper half of Fig. 2). A different situation can be observed for the interaction of e-core mutant with PC:PS membrane. In this case the holes are about 2 nm deep, with much large widths (about 80–120 nm) and elevations of both types appear over the entire bilayer surface (see Fig. 3). The elevations in the vicinities of holes are large and can reach heights of 3–4 nm. At the same time one can observe also corrugations similar to those seen for the ecto-domain.

As the reaction proceeds, the core mutant produces large wide holes possessing a depth of 4 nm, but regions of intact membrane can still be resolved (see Fig. 4). The membrane elevations range up to 4 nm height. At the same time there are also relatively flat regions elevated by 1–2 nm at the later stages of core mutant interaction with PC:PS bilayer. The membrane state in advanced stages of the interaction with the ecto-domain is different from the case of the core mutant. All surfaces of the membrane exhibit nanoscale remodeling, leading to a net-like appearance (see Fig. 5). Total remodeling of the PC:PS bilayer also occurrs in interaction with the e-core mutant. But in this case, extensive corrugation is seen, with protrusions above the remaining membrane surface of up to 8 nm height, and holes of 4 nm depth indicating complete bilayer removal (see Fig. 6).

The tendency toward wide or narrow holes can be discussed in terms of the mechanism of small hole coalescence. The initial holes produced by a single protein are very small and could be refilled by neighboring lipid molecules to disappear, or unite with other holes producing larger and growing holes. In these systems, we have observed the characteristic differences in the holes sizes for the different proteins at all stages of interaction. A possible explanation of these differences is a participation or influence of the specific protein (full ecto-domain, core mutant or e-core mutant) on the process of small, unit holes coalescence due to local energetics. Energetics could also

Fig. 7. Comparison of the kinetics for the three protein types with negatively charged membrane, presented on identical scales. Quantification of membrane destruction is represented by rms roughness of the surface. Plotting this parameter as a function of time yielded the kinetic curve. Each point is an average of four images, standard deviations indicated by error bar. Membrane roughness starting 50 min scanning time before adding the mutant ('negative' time) is included to show that changes occurred only after addition of protein (time 0 represents first image after this addition, approximately 5 min after protein addition). (a) Kinetics of PC:PS membrane destruction by e-core mutant. (b) Kinetics of PC:PS membrane destruction by ectodomain. (c) Kinetics of PC:PS membrane destruction by core mutant.

control the appearance of membrane elevations of different shapes and sizes. On the other hand, the different types of observed deposits on top of the membrane could be due to a different phenomenon. The large bumps could be attributed to clumps of lipid molecules leaving the membrane and settling randomly on the surface. This could explain the variable heights of these elevations. But flat low elevations could be attributed to membrane blistering [39]. In this case the negatively charged lipids could be repelled and lifted up from the mica, possessing low negative charge.

As was pointed out in Section 3.4, the kinetics of membrane destruction is also different for full gp41 ecto-domain and the two mutants. The kinetic results show that the proteins containing the fusion peptide lead to more complete membrane disruption, as noted by the saturation rms values. Thus, the core mutant has the slowest rise time, and lowest (approx 0.7 nm rms) saturation roughness. The large ultimate rms value for the e-core (2 nm rms) appears from the images to be due to the accumulation of material, presumably membrane lipids, near the edges of holes which could be due to hydrophobic interactions in the aqueous medium. Observed differences in the rate of membrane destruction could be attributed to the influence of a specific protein (full ecto-domain, core mutant or e-core mutant) on the kinetic parameters of the membrane reorganization process. There could be different mechanisms of this influence that is partially confirmed by the pointed difference in the 'effectiveness' between three proteins studied. There is also a remarkable steep increase in the rate of membrane destruction over a relatively narrow time interval for the e-core mutant. This could point to the existence of 'lag-burst' type kinetics for this protein. All the discussed features actually refer to the basic question: are the modes of interaction between studied proteins and negatively charged lipid bilayers synergistic (cooperative) or random and could be a challenge for further studies.

5. Conclusions

In this work we report direct observation by AFM of the process of interaction between three proteins – ecto-domain of HIV envelope protein gp41 and its two truncated forms in the post-fusion state, and 2 lipid bilayers – zwitterionic and negatively charged. Real-time imaging with nanometer resolution enabled a confirmation that all three proteins strongly perturb the negatively charged lipid membrane and do not affect the zwitterionic membrane. The use of AFM allowed tracking and describing the nanoscale changes in the membrane integrity in real time obtaining access to the fine details of the interaction process. Furthermore we suggest a quantitative approach to characterize the kinetics of these interactions and described the differences and features in the kinetics for the three proteins.

Acknowledgements

This study was supported by the Israel Science Foundation. Y.S. is the incumbent of the Harold S. and Harriet B. Brady Professorial Chair in Cancer Research.

References

[1] B.P. Jena, J.K.H. Hörber, Atomic force microscopy in cell biology, Methods in Cell Biology, Academic Press, San Diego, CA, 2002.
[2] A. Engel, D.J. Muller, Observing single biomolecules at work with the atomic force microscope, Nat. Struct. Biol. 7 (2000) 715–718.
[3] M.-C. Giocondi, V. Vié, E. Lesniewska, P.-E. Milhiet, M. Zinke-Allmang, C. Le Grimellec, Phase topology and growth of single domains in lipid bilayers, Langmuir 17 (2001) 1653–1659.
[4] V. Vie, N. Van Mau, E. Lesniewska, J.P. Goudonnet, F. Heitz, C. Le Grimellec, Distribution of ganglioside GM1 between two-component, two-phase phosphatidylcholine monolayers, Langmuir 14 (1998) 4574–4583.
[5] H.A. Rinia, J.W. Boots, D.T. Rijkers, R.A. Kik, M.M. Snel, R.A. Demel, J.A. Killian, J.P. van der Eerden, B. de Kruijff, Domain formation in phosphatidylcholine bilayers containing transmembrane peptides: specific effects of flanking residues, Biochemistry 41 (2002) 2814–2824.
[6] K. El Kirat, L. Lins, R. Brasseur, Y.F. Dufrene, Fusogenic tilted peptides induce nanoscale holes in supported phosphatidylcholine bilayers, Langmuir 21 (2005) 3116–3121.
[7] K. El Kirat, Y.F. Dufrene, L. Lins, R. Brasseur, The SIV tilted peptide induces cylindrical reverse micelles in supported lipid bilayers, Biochemistry 45 (2006) 9336–9341.
[8] P.E. Milhiet, M.C. Giocondi, O. Baghdadi, F. Ronzon, B. Roux, C. Le Grimellec, Spontaneous insertion and partitioning of alkaline phosphatase into model lipid rafts, EMBO Rep. 3 (2002) 485–490.
[9] T. Puntheeranurak, C. Stroh, R. Zhu, C. Angsuthanasombat, P. Hinterdorfer, Structure and distribution of the *Bacillus thuringiensis* Cry4Ba toxin in lipid membranes, Ultramicroscopy 105 (2005) 115–124.
[10] R. Gamsjaeger, A. Johs, A. Gries, H.J. Gruber, C. Romanin, R. Prassl, P. Hinterdorfer, Membrane binding of beta(2)-glycoprotein I can be described by a two-state reaction model: an atomic force microscopy and surface plasmon resonance study, Biochem. J. 389 (2005) 665–673.
[11] K. El Kirat, V. Duprès, Y.F. Dufrêne, Blistering of supported lipid membranes induced by phospholipase D, as observed by real-time atomic force microscopy, Biochim. Biophys. Acta–Biomembranes 1778 (2008) 276–282.
[12] N. Lev, Y. Shai, Fatty acids can substitute the HIV fusion peptide in lipid merging and fusion: an analogy between viral and palmitoylated eukaryotic fusion proteins, J. Mol. Biol. 374 (2007) 220–230.
[13] J.M. Coffin, Genetic variation in AIDS viruses, Cell 46 (1986) 1–4.
[14] E.O. Freed, M.A. Martin, The role of human immunodeficiency virus type 1 envelope glycoproteins in virus infection, J. Biol. Chem. 270 (1995) 23883–23886.
[15] N.W. Douglas, G.H. Munro, R.S. Daniels, HIV/SIV glycoproteins: structure–function relationships, J. Mol. Biol. 273 (1997) 122–149.
[16] D.C. Chan, P.S. Kim, HIV entry and its inhibition, Cell 93 (1998) 681–684.
[17] M. Kowalski, J. Potz, L. Basiripour, T. Dorfman, W.C. Goh, E. Terwilliger, A. Dayton, C. Rosen, W. Haseltine, J. Sodroski, Functional regions of the envelope glycoprotein of human immunodeficiency virus type 1, Science 237 (1987) 1351–1355.
[18] F.D. Veronese, A.L. DeVico, T.D. Copeland, S. Oroszlan, R.C. Gallo, M.G. Sarngadharan, Characterization of gp41 as the transmembrane protein coded by the HTLV-III/LAV envelope gene, Science 229 (1985) 1402–1405.
[19] R. Wyatt, J. Sodroski, The HIV-1 envelope glycoproteins: fusogens, antigens, and immunogens, Science 280 (1998) 1884–1888.
[20] W. Weissenhorn, A. Dessen, L.J. Calder, S.C. Harrison, J.J. Skehel, D.C. Wiley, Structural basis for membrane fusion by enveloped viruses, Mol. Membr. Biol. 16 (1999) 3–9.
[21] D.M. Eckert, P.S. Kim, Mechanisms of viral membrane fusion and its inhibition, Annu. Rev. Biochem. 70 (2001) 777–810.
[22] D.C. Chan, D. Fass, J.M. Berger, P.S. Kim, Core structure of gp41 from the HIV envelope glycoprotein, Cell 89 (1997) 263–273.
[23] R.A. Furuta, C.T. Wild, Y. Weng, C.D. Weiss, Capture of an early fusion-active conformation of HIV-1 gp41, Nat. Struct. Biol. 5 (1998) 276–279.
[24] I. Munoz-Barroso, S. Durell, K. Sakaguchi, E. Appella, R. Blumenthal, Dilation of the human immunodeficiency virus-1 envelope glycoprotein fusion pore revealed by the inhibitory action of a synthetic peptide from gp41, J. Cell. Biol. 140 (1998) 315–323.
[25] K. Salzwedel, J.T. West, E. Hunter, A conserved tryptophan-rich motif in the membrane-proximal region of the human immunodeficiency virus type 1 gp41 ectodomain is important for Env-mediated fusion and virus infectivity, J. Virol. 73 (1999) 2469–2480.
[26] I. Munoz-Barroso, K. Salzwedel, E. Hunter, R. Blumenthal, Role of the membrane-proximal domain in the initial stages of human immunodeficiency virus type 1 envelope glycoprotein-mediated membrane fusion, J. Virol. 73 (1999) 6089–6092.
[27] S.G. Peisajovich, R.F. Epand, M. Pritsker, Y. Shai, R.M. Epand, The polar region consecutive to the HIV fusion peptide participates in membrane fusion, Biochemistry 39 (2000) 1826–1833.
[28] T. Suarez, W.R. Gallaher, A. Agirre, F.M. Goni, J.L. Nieva, Membrane interface-interacting sequences within the ectodomain of the human immunodeficiency virus type 1 envelope glycoprotein: putative role during viral fusion, J. Virol. 74 (2000) 8038–8047.
[29] K. Sackett, Y. Shai, The HIV-1 gp41 N-terminal heptad repeat plays an essential role in membrane fusion, Biochemistry 41 (2002) 4678–4685.
[30] Y. Wexler-Cohen, K. Sackett, Y. Shai, The role of the N-terminal heptad repeat of HIV-1 in the actual lipid mixing step as revealed by its substitution with distant coiled coils, Biochemistry 44 (2005) 5853–5861.
[31] O. Korazim, K. Sackett, Y. Shai, Functional and structural characterization of HIV-1 gp41 ectodomain regions in phospholipid membranes suggests that the fusion-active conformation is extended, J. Mol. Biol. 364 (2006) 1103–1117.
[32] R. Pascual, M.R. Moreno, J. Villalain, A peptide pertaining to the loop segment of human immunodeficiency virus gp41 binds and interacts with model biomembranes: implications for the fusion mechanism, J. Virol. 79 (2005) 5142–5152.

[33] R. Pascual, M. Contreras, A. Fedorov, M. Prieto, J. Villalain, Interaction of a peptide derived from the N-heptad repeat region of gp41 Env ectodomain with model membranes. Modulation of phospholipid phase behavior, Biochemistry 44 (2005) 14275–14288.
[34] M.R. Moreno, M. Giudici, J. Villalain, The membranotropic regions of the endo and ecto domains of HIV gp41 envelope glycoprotein, Biochim. Biophys. Acta 1758 (2006) 111–123.
[35] Y. Kliger, S.G. Peisajovich, R. Blumenthal, Y. Shai, Membrane-induced conformational change during the activation of HIV-1 gp41, J. Mol. Biol. 301 (2000) 905–914.
[36] R.M. Markosyan, F.S. Cohen, G.B. Melikyan, HIV-1 envelope proteins complete their folding into six-helix bundles immediately after fusion pore formation, Mol. Biol. Cell 14 (2003) 926–938.
[37] N. Lev, Y. Fridmann-Sirkis, L. Blank, A. Bitler, R.F. Epand, R.M. Epand, Y. Shai, Conformational stability and membrane interaction of the full-length ectodomain of HIV-1 gp41: implication for mode of action, Biochemistry 48 (2009) 3166–3175.
[38] J.D. Kiely, D.A. Bonnell, Quantification of topographic structure by scanning probe microscopy, J. Vac. Sci. Technol. B 15 (1997) 1483–1493.
[39] H.A. Rinia, R.A. Demel, J.P.J.M. van der Erden, B. de Kruijff, Blistering of Langmuir–Blodgett bilayers containing anionic phospholipids as observed by atomic force microscopy, Biophys. J. 77 (1999) 1683–1693.